Nuclear Materials and Energy 18 (2019) 193–200

Contents lists available at ScienceDirect

Nuclear Materials and Energy

journal homepage: www.elsevier.com/locate/nme

Statistical properties of the plasma fluctuations and turbulent cross-field fluxes in the outboard mid-plane scrape-off layer of Alcator C-Mod

R. Kube[*,a], O.E. Garcia[a], A. Theodorsen[a], A.Q. Kuang[b], B. LaBombard[b], J.L. Terry[b], D. Brunner[c]

[a] Department of Physics and Technology, UiT The Arctic University of Norway, Tromsø N-9037, Norway
[b] MIT Plasma Science and Fusion Center, Cambridge, MA 02139, United States
[c] Commonwealth Fusion Systems, Cambridge, MA, 02139, United States

A B S T R A C T

The Alcator C-Mod mirror Langmuir probe diagnostic is used to characterize plasma fluctuations in the outboard mid-plane scrape-off layer (SOL). Ohmically heated L-mode plasmas with Greenwald fractions from 0.1 to 0.45 are analyzed. In plasmas with a low line-averaged core density, the radial profiles of the average electron density and temperature feature a two-scale structure with a strong gradient in the near-SOL and a weak gradient in the far-SOL. The relative fluctuation levels of the electron density are below 25% throughout the entire SOL and the fluctuation driven heat flux is dominated by plasma density fluctuations. In the plasma with the highest line-averaged core density, the radial profiles of the electron density and temperature feature only a single weak gradient length scale across the SOL. The plasma density at the limiter radius is approximately 10 times larger than in low-density discharges. The average electron temperature at the separatrix falls to approximately 30 eV while the magnitude of the relative temperature fluctuations increases with the line-averaged core plasma density. With increasing plasma density, the fluctuation-driven heat fluxes increase by more than one order of magnitude while retaining a relative fluctuation level of approximately 3. Even though the SOL is on average cooler than in low density discharges, large electron temperature fluctuations govern the turbulence driven heat flux towards the wall while contributions from density fluctuations and triple correlations contribute approximately 35% and 15%, respectively.

1. Introduction

As the power exhaust channel for tokamak plasmas, the scrape-off layer (SOL) distributes plasma fluxes coming from inside the last closed flux surface onto material surfaces [1]. It is widely believed that competition between parallel and cross-field transport determines the scale lengths of radial profiles in the SOL [2–8]. As plasma and heat crosses the separatrix and enters the SOL, parallel transport immediately disperses it along the magnetic field lines into the divertor region. Acoustic streaming governs the parallel transport of plasma density while heat transport along the field lines is believed to be governed by thermal conduction [9,10]. Cross-field transport in the SOL is dominated by the radial motion of so-called plasma blobs [5,11–14]. In order to establish predictive modeling capabilities for expected heat loads on plasma facing components in reactor relevant conditions, the scaling of both the parallel and perpendicular transport mechanisms with the relevant plasma parameters needs to be understood.

Blobs are field-aligned structures of elevated pressure which appear strongly localized when viewed in the radial-poloidal plane. They present order unity perturbations to the background particle density and temperature, and the magnitude of the radial transport they mediate depends on their pressure amplitude as well as their cross-field size [12,15–20]. Theoretical work on blob propagation suggests that their radial velocity depends sensitively on the plasma collisionality [7,21,22]. In low collisionality plasmas, blobs may extend along magnetic field lines all the way to electric sheaths at the divertor plate. This effectively dissipates electric drift vorticity generated by the blobs, thereby impeding their radial propagation [12,17]. In high collisionality plasmas, this dissipation channel is rendered ineffective by parallel resistivity such that blobs would propagate faster than for low collisionality plasmas [8,23–25]. Experimentally, the collisionality of the SOL plasma can be controlled by the line-averaged core plasma density. Recent theoretical and experimental work suggests that particle density time series sampled in SOL plasmas are well described as a super-position of uncorrelated pulses, where each pulse is due to the radial propagation of a plasma blob [26–32].

In the situation where parallel transport dominates cross-field transport, small gradient scale lengths of the average plasma density and temperature profiles are expected in the SOL. In the opposite situation, it is expected that the scale lengths become larger, exposing the main chamber wall to, on average, a hotter and denser plasma. However, SOL plasmas are characterized by order unity fluctuations of these plasma parameters. Recognizing that the SOL plasmas is well described as a non-linear system which features turbulent flows driven by these large-amplitude fluctuations [33–36], it is desirable to characterize the fluctuations of the plasma and the radial fluxes in the same

* Corresponding author
E-mail address: ralph.kube@uit.no (R. Kube).

https://doi.org/10.1016/j.nme.2018.11.021
Received 31 July 2018; Received in revised form 22 November 2018; Accepted 23 November 2018

manner as has been done for average profiles.

This contribution revisits the dependence of fluctuation driven cross-field transport in the scrape-off layer plasma on the line-averaged core-plasma density [4,6,8,25,33,37–39]. Utilizing Mirror Langmuir Probes (MLP) installed in the low-field side, outboard mid-plane reciprocating probe diagnostic, the electron density, electron temperature, and the plasma potential are sampled on a time scale smaller than the timescale of the turbulent SOL flows. Here we use this capability to compile radial profiles of the lowest order statistical moments for the electron density, the electron temperature, the radial velocity, and for the fluctuation driven particle and heat fluxes. This unique sampling capability of the MLP allows the characterization of just the fluctuation statistics of the fluctuation driven fluxes in the SOL and their dependence on the line-averaged plasma density.

2. Experimental setup

The SOL plasma in Alcator C-Mod has been investigated for several ohmically heated, lower single-null diverted plasma discharges. In each discharge the line-averaged core plasma density was held at a constant value $\bar{n}_e/n_G = 0.13, 0.22, 0.28$ and 0.45, where n_G denotes the Greenwald density [40]. All figures presented in this paper encode the line-averaged core plasma density using the color map given in Fig. 1.

All discharges were performed at a constant poloidal current of approximately 0.55 MA at the flat top which leads to a comparable magnetic geometry for all the discharges. Fig. 2 shows the magnetic equilibrium, as reconstructed using EFIT [41]. Fig. 3 shows the connection length from the horizontal scanning probe, counter-clockwise along the magnetic field lines, onto material targets. Here, ρ denotes the distance to the separatrix as mapped to the outboard mid-plane location. In the region $\rho \lesssim 1.5$ cm the field lines intersect the lower divertor stack. In the region $\rho \gtrsim 1.5$ cm the field lines intersect a poloidal limiter structure, resulting in shorter connection lengths. Data for this region is omitted from the figure.

The horizontal scanning probe [42] was equipped with a Mach probe head [43], whose four electrodes were each connected to an MLP [31,44,45]. The four electrodes are arranged in a pyramidal geometry and labelled NE (north-east), SE (south-east), SW (south-west), and NW (north-west), according to their location relative to the other electrodes. Fig. 4 shows the layout of the electrodes on the probe head and relative to the magnetic field. This probe is located approximately 10 cm above the outboard mid-plane location. In the analysis presented here, data from between one to three probe plunges during stationary plasma parameters is used.

Traditional Langmuir probes sample radial profiles of the estimated average electron density n_e and the average electron temperature T_e by applying a sweeping bias voltage. To avoid hysteresis effects, the frequency of the sweeping bias voltage is limited to frequencies below the characteristic time scale of turbulent flows in the SOL plasma [46]. This mode of operation assumes a constant background plasma during the sweep. Another commonly employed method for operating Langmuir probes is to bias them negatively such that they sample the ion saturation current I_s. Sampling on a frequency below the characteristic time scale of the turbulent flows in the SOL allows to compute lower order statistics of I_s time series, such as the average $\langle I_s \rangle$, the root-mean-square value $I_{s,\,rms}$, as well as coefficients of skewness and excess kurtosis, defined respectively by $S_{I_s} = \langle((I_s - \langle I_s\rangle)/I_{s,rms})^3\rangle$ and $F_{I_s} = \langle((I_s - \langle I_s\rangle)/I_{s,rms})^4\rangle - 3$. Asymmetric distributions of fluctuations where a significant number of samples exceed the average value generally feature positive values of both S and F.

Fig. 1. Color encoding of $\bar{n}_e/n_G$ used in Figs. 2–10.

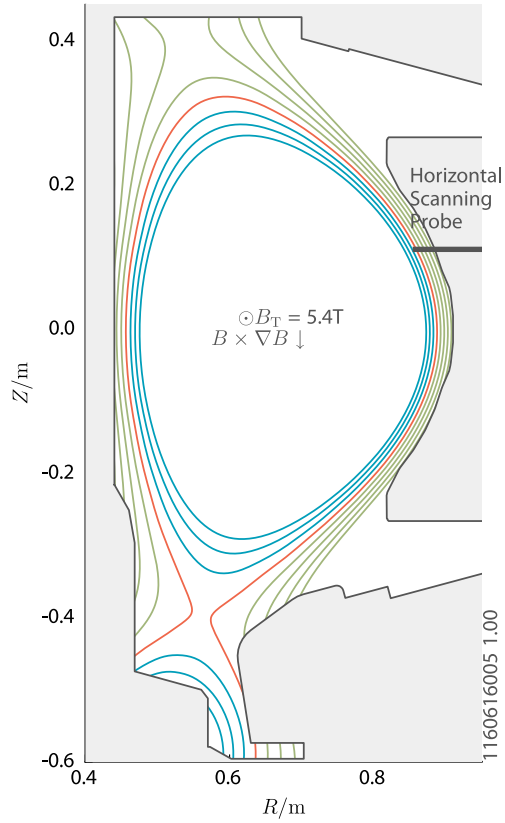

Fig. 2. Reconstructed magnetic flux surfaces. Open magnetic field lines, intersecting the poloidal limiter structure or the divertor structure are shown in green. The magnetic separatrix is drawn in red and the trajectory of the scanning probe is denoted by the black vertical line. (For interpretation of the references to colour in this figure legend, the reader is referred to the web version of this article.)

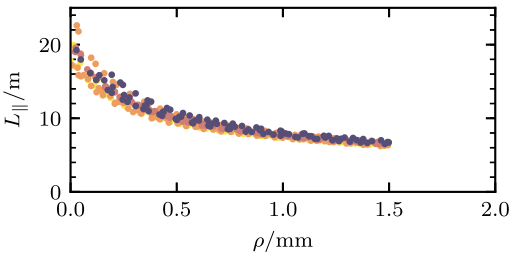

Fig. 3. Radial profile of the distance from the probe position to the lower divertor stack when following the magnetic field lines counter-clockwise.

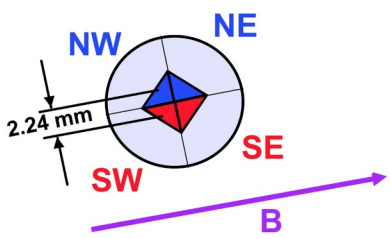

Fig. 4. Layout of the probe head installed on the scanning probe, viewing from inside the plasma.

MLPs sample the electron density, temperature and the plasma potential in real time. This allows the compilation of all the lowest order statistical moments of these quantities. Practically, they combine the sweeping voltage and negative bias mode of operation of Langmuir probes. To do so, the MLP bias drive applies a fast-switching voltage to

a Langmuir electrode on a sub-microsecond time scale. By dynamically updating the voltage states as to cover a sufficiently large voltage range, the MLP system infers the electron density n_e, the electron temperature T_e, and the plasma potential V_p by fitting a current-voltage characteristic on this data. From this data, a more complete picture of the fluctuation-driven transport in the SOL plasma can be obtained.

Estimators for the radial electric drift velocity as well as for the fluctuation driven particle and heat fluxes are defined by

$$U = \frac{1}{2}\frac{(V_p^{SE} + V_p^{SW}) - (V_p^{NE} + V_p^{NW})}{\triangle_z B(R+a)}, \tag{1}$$

$$\hat{\Gamma}_n = \tilde{U}\tilde{n}_e, \tag{2}$$

$$\hat{\Gamma}_T = \tilde{U}\tilde{n}_e\frac{\langle T_e\rangle}{T_{e,\mathrm{rms}}} + \tilde{U}\tilde{T}_e\frac{\langle n_e\rangle}{n_{e,\mathrm{rms}}} + \tilde{U}\tilde{n}_e\tilde{T}_e. \tag{3}$$

These are readily evaluated using the data reported by the MLP. Here $\triangle_z = 2.2\,\mathrm{mm}$ denotes the vertical distance between the north and south electrode groups, $R = 0.68\,\mathrm{m}$ and $a = 0.22\,\mathrm{m}$ denote the major and minor radius respectively, and $B(R+a) \approx 4.1\,\mathrm{T}$ gives the toroidal magnetic field at the probe location. Fluctuating quantities are denoted by $\tilde{\Phi} = (\Phi - \langle\Phi\rangle)/\Phi_{\mathrm{rms}}$. The fluctuation-driven electron heat flux is comprised of a convective part, driven by electron density fluctuations, a conductive part, driven by electron temperature fluctuations, and of a part due to triple correlations.

3. Fluctuation profiles

Fig. 5 shows radial profiles of the lowest order statistical moments for I_s, n_e and T_e. The gray area denotes the approximate location of the limiter shadow. The radial profiles of the average ion saturation current, shown in the top panel of the left column, decay approximately exponentially. For $\bar{n}_e/n_G \lesssim 0.3$, a two-scale structure is observed, with a strong gradient in the near-SOL and a weak gradient in the far-SOL. Profiles sampled in the high-density discharges with $\bar{n}_e/n_G \approx 0.45$ show no visible distinction between a near-SOL and a far-SOL region. In the lowest density discharges, the relative fluctuation level increases from 0.25 at the separatrix to 0.5 at $\rho \approx 2$cm. For $\bar{n}_e/n_G \approx 0.45$, the relative fluctuation level is approximately 0.5 throughout the entire SOL. Radial profiles of skewness S and excess kurtosis F show similar trends as the relative fluctuation level. Both, S and F increase only slightly with ρ, however both S and F are significantly larger in the discharge with $\bar{n}_e/n_G = 0.45$ than in lower density discharges.

Profiles of the average electron density, shown in the top row of the middle column, appear qualitatively similar to the $\langle I_s\rangle$ profiles. A two-scale structure with a strong gradient in the near-SOL and a weak gradient in the far-SOL are distinguishable in discharges with $\bar{n}_e/n_G \lesssim 0.3$. In the high density discharge, the profiles feature an approximately uniform gradient length scale which is larger than in the lowest density discharge. At the limiter radius, $\langle n_e\rangle$ is larger by a factor of 10 than in the lowest density discharge. Radial profiles of the relative fluctuation level, skewness and excess kurtosis show little variation with ρ and $\bar{n}_e/n_G$. The relative fluctuation level is approximately $0.15 - 0.25$ throughout the SOL and increases slightly with ρ in discharges with $\bar{n}_e/n_G \lesssim 0.3$. Coefficients of skewness and excess kurtosis are small, S, $F \lesssim 1$, and are constant throughout the SOL.

The radial profiles of the average electron temperature are qualitatively different from those of the electron density. While both profiles decrease monotonically with ρ, the average electron temperature decreases with increasing $\bar{n}_e/n_G$. At the separatrix we find $\langle T_e(0)\rangle \approx 60\,\mathrm{eV}$ in discharges with $\bar{n}_e/n_G \lesssim 0.3$. In the high density discharge we find $\langle T_e(0)\rangle \approx 30\,\mathrm{eV}$. The radial profiles of the relative fluctuation level show a strong dependence on the line-averaged core plasma density and little sensitivity on ρ. For $\bar{n}_e/n_G \lesssim 0.3$, $T_{e,\ \mathrm{rms}}/\langle T_e\rangle$ is given by approximately $0.15 - 0.25$, while for $\bar{n}_e/n_G \approx 0.45$ the relative fluctuation level is approximately 0.5; larger by a factor of two. Similarly, T_e features larger profile values for skewness and excess kurtosis in the high density discharge, which suggests an abundance of temperature fluctuations which significantly exceed the average temperature.

In order to quantify the dependence of the average profile gradient scale length on $\bar{n}_e/n_G$, the function

$$\langle\Phi\rangle(\rho) = \begin{cases} \sim\exp\left(-\dfrac{\rho}{L_n}\right) & \text{for } \rho \le \rho_b \\ \sim\exp\left(-\dfrac{\rho}{L_f}\right) & \text{for } \rho > \rho_b \end{cases} \tag{4}$$

is fitted on the data shown in the row second from the top of Fig. 5for $0 < \rho < 1.5\,\mathrm{cm}$ using a least-squares method. These fits are shown in Fig. 6. The near- and far-SOL profile scale lengths are denoted by L_n and L_f respectively, and ρ_b denotes the break point between the two regions. The ion saturation current, electron density, and temperature profiles feature profile length scales given by L_n between 0.5 and 1 cm. The far-

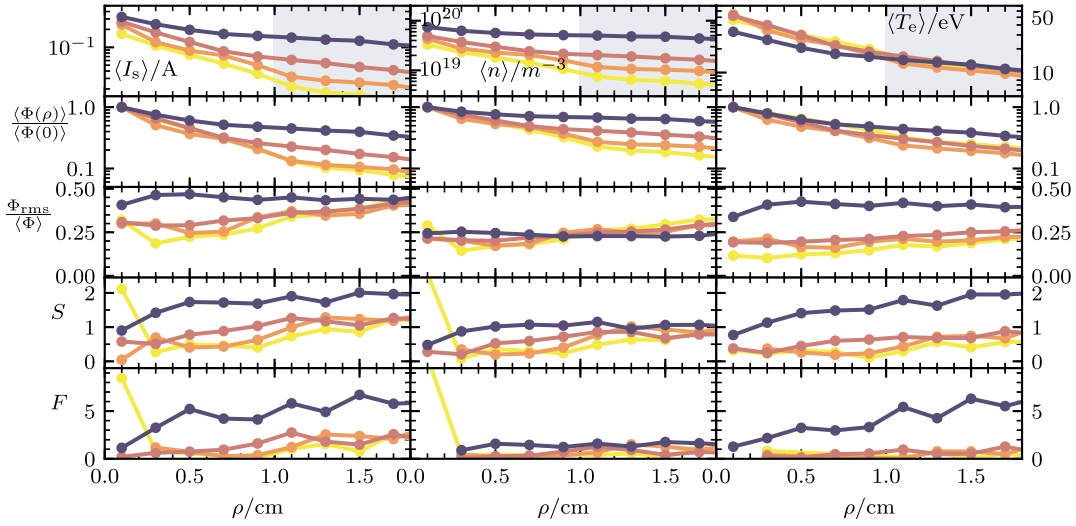

Fig. 5. Radial profiles of the lowest order statistical moments for the ion saturation current (left column), electron density (middle column), and the electron temperature (right column). The gray area denotes the approximate location of the limiter shadow. The top row shows the average value, the second to top row shows the profile of the average value relative to the value at the separatrix, $\rho = 0$. The middle row shows the relative fluctuation level and the two lowermost rows show radial profiles of the sample skewness and excess kurtosis.

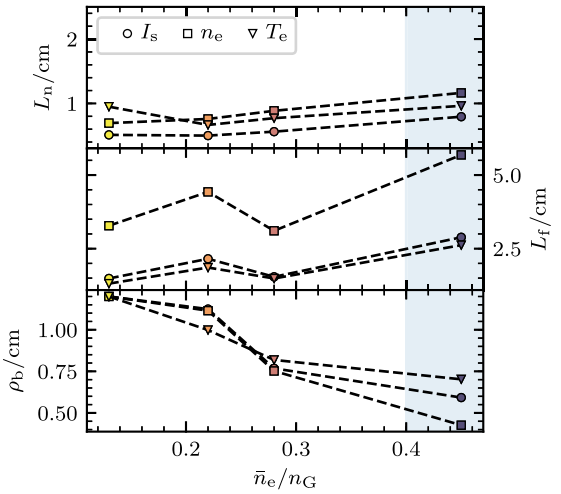

Fig. 6. Length scales of the near-SOL (upper panel), far-SOL (middle panel) and the position of the break point between near- and far-SOL (lower panel). The colored area denotes detached divertor conditions.

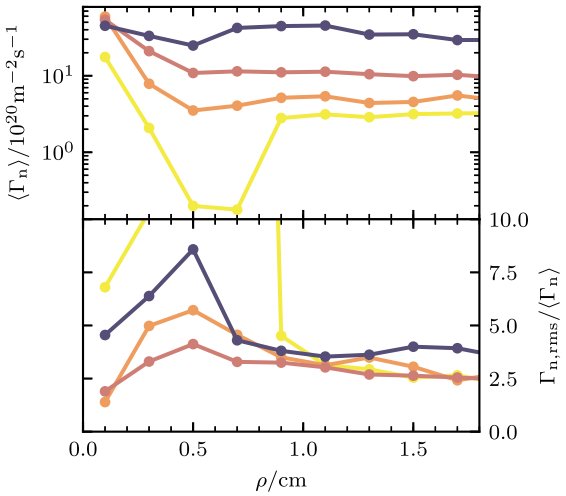

Fig. 8. Profiles of the average particle flux (upper panel) and its relative fluctuation level (lower panel).

SOL profile scale lengths for I_s and T_e are approximately 2 cm. For n_e, we find $L_f \approx 3-4$ cm and for the high density discharge with $\bar{n}_e/n_G \approx 0.45$ we find $L_f \approx 5.5$ cm. For all three profiles, the break point moves towards the separatrix, from $\rho \approx 1$cm in low density discharges to $\rho \approx 0.5$cm in high density discharges. Given the radial resolution of the sampled profiles, the distinction between a near- and a far-SOL appears artificial in the high-density discharges.

Fig. 7 shows radial profiles of the root-mean square value, skewness and excess kurtosis calculated for estimators of the radial velocity given by Eq. 1 using both the floating potential $\tilde{U}_{V_f}$ and the plasma potential $\tilde{U}_{V_p}$. For $\bar{n}_e/n_G \lesssim 0.3$, $\tilde{U}_{V_f,\mathrm{rms}}$ decreases with ρ, from approximately $700-1000\,\mathrm{ms}^{-1}$ at $\rho \approx 3$ mm to approximately $400\mathrm{ms}^{-1}$ at $\rho = 2$ cm. For $\bar{n}_e/n_G \gtrsim 0.3$, $\tilde{U}_{V_f}$ is given by approximately $600\,\mathrm{ms}^{-1}$ at the separatrix and decreases weakly radially outward. Independent of $\bar{n}_e/n_G$ and ρ, estimators for skewness and excess kurtosis are negligibly small, suggesting normally distributed fluctuations.

For $\bar{n}_e/n_G \lesssim 0.3$, radial profiles of $\tilde{U}_{V_p,\mathrm{rms}}$ are comparable to the profiles calculated from $\tilde{U}_{V_f,\mathrm{rms}}$. Root-mean square values sampled in the high density discharge on the other hand are significantly larger than in the low density discharges, approximately $1000\,\mathrm{ms}^{-1}$. Furthermore, coefficients of sample skewness and excess kurtosis are also significantly larger than found when using the floating potential to estimate the radial velocity. While estimators for S and F obtained for the discharges with $\bar{n}_e/n_G \lesssim 0.3$ cluster, these estimators are significantly larger in the highest density discharge. An explanation for these large sample coefficients is an abundance of velocity samples exceeding the root-mean-square value. Velocity samples of this magnitude are not measured by the estimator using the floating potential.

Fig. 8 shows the profiles of the radial particle flux. Profiles of $\langle\Gamma_n\rangle$ are flat throughout the SOL for $\rho \gtrsim 0.5$mm. However, the data sampled in the low density discharge with $\bar{n}_e/n_G = 0.12$ shows large uncertainties, especially in between $\rho = 0.5$ cm and 1 cm. The magnitude of the particle flux increases monotonously with $\bar{n}_e/n_G$ from approximately $5 \times 10^{20}\,\mathrm{m}^{-2}\mathrm{s}^{-1}$ for $\bar{n}_e/n_G = 0.22$ to more than $3 \times 10^{21}\,\mathrm{m}^{-2}\mathrm{s}^{-1}$ for $\bar{n}_e/n_G = 0.45$. On the other hand, the length scale of the average plasma density profile in the near-SOL remains constant and L_f varies by less than a factor of two. This further corroborates the idea that the radial particle transport in the SOL is not well described by flux-gradient expressions [38,47]. Similar to the average value, the relative fluctuation level of the radial particle flux is approximately constant for $\rho \gtrsim 0.5$ cm. It varies in the range $2-5$, independent of the line-averaged core plasma density.

Fig. 9 shows the profiles of the average heat fluxes due to conduction (left column), convection (middle column) and triple correlations (right column) and their respective relative fluctuation level (bottom row). We note here that the electron heat flux at the separatrix, $\rho = 0$ cm, is approximately $0.1\,\mathrm{MWm}^{-2}$. Assuming the same amount is carried by the ions, approximately $0.2\,\mathrm{MWm}^{-2}$ enter the SOL. Further assuming that this heat flux is constant over a 0.2 m strip, centered

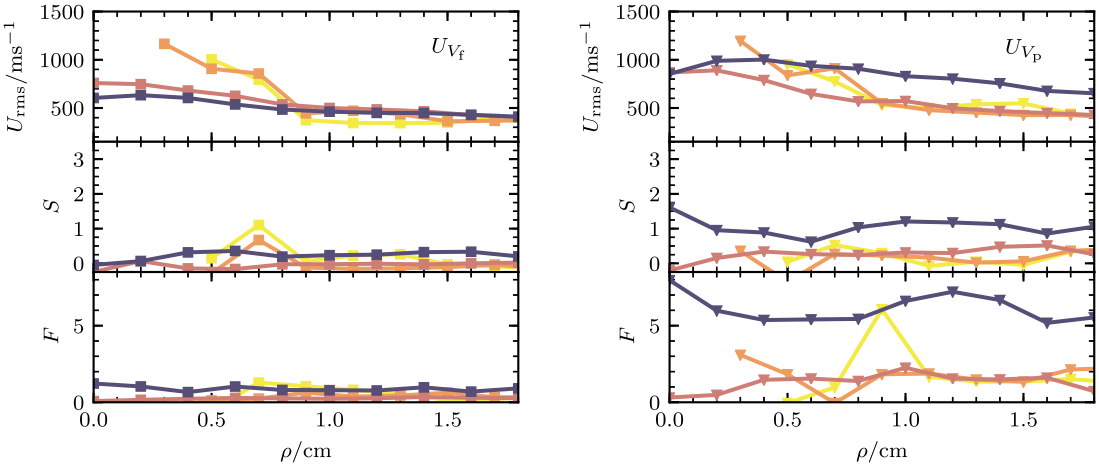

Fig. 7. Profiles of the lower order statistical moments for the radial velocity, estimated using V_f (left panels) and V_p (right panels).

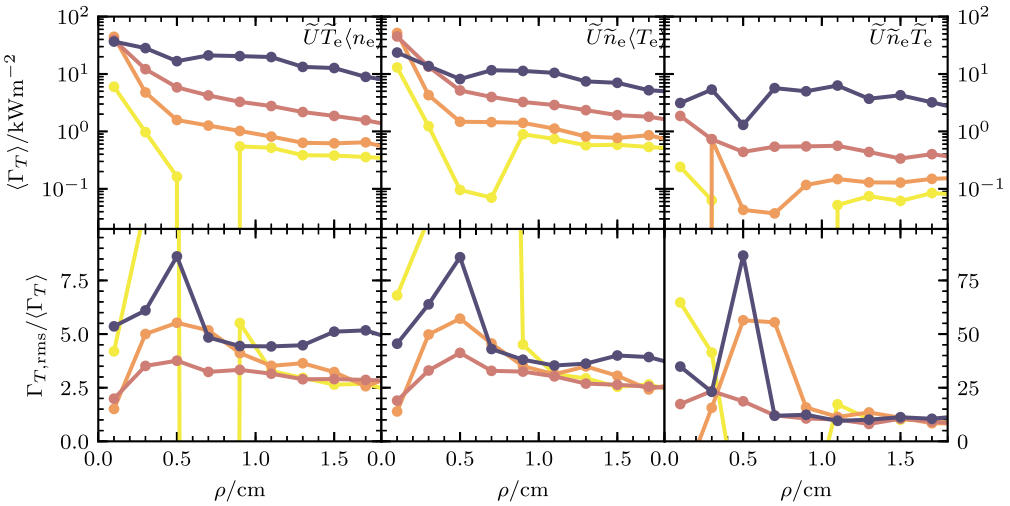

Fig. 9. Profiles of conductive heat flux (left column), the convective heat flux (middle column) and the heat flux driven by triple correlations (right column). The upper row shows the average value and the lower row shows the relative fluctuation level.

around the outboard mid-plant location, the total heat flowing into the SOL amounts to approximately 0.2 MW. For L-mode discharges with similar magnetic equilibrium and core-plasma densities as those investigated here, $P_{\mathrm{Ohmic}} - P_{\mathrm{rad}}$ is approximately 0.3 MW, where P_{Ohmic} is the ohmic heating power and P_{rad} is the power radiated from the central plasma column [48]. That is, the magnitude of the heat fluxes shown in Fig. 9 agrees with the global power balance estimate within one order of magnitude.

Similar to the profiles of the particle flux, all average heat fluxes are nearly flat throughout the SOL and their magnitude increases with the plasma line-averaged core density. We find significant dips of the average profiles in the near-SOL, $\rho \lesssim 1$cm in the lowest density discharge with $\overline{n}_e/n_G = 0.12$, as well as a dip in the triple correlation heat flux for a discharge with $\overline{n}_e/n_G = 0.22$. The relative fluctuation level of the heat fluxes shows a more complicated behavior. For the conductive and convective heat flux, we find that it is between 2 and 7 times the average value and that it increases slightly with $\overline{n}_e/n_G$. For the triple correlations, we find significantly larger relative fluctuation levels.

Fig. 10 shows the relative magnitude of the profile-averaged fluctuation driven heat fluxes. In discharges with $\overline{n}_e/n_G \lesssim 0.3$, the radial heat flux is governed by convection, driven by density fluctuations,

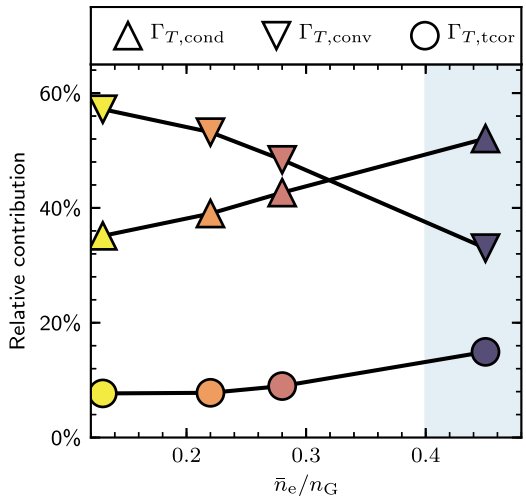

Fig. 10. Relative contribution of the conductive, convective and triple correlation heat flux to the total fluctuation driven heat flux.

which contribute nearly 60% to the total heat flux. In the high-density discharge more than 50% of the total heat flux is due to conduction, driven by temperature fluctuations. In this dense plasma, convection contributes approximately 35% and triple correlations contribute approximately 15% to the total heat flux.

In order to investigate the origin of the heat flux switching from convection to conduction dominated, we continue by discussing the correlations of $\tilde{n}_e$, $\tilde{T}_e$, and $\tilde{U}$. For this, data from 3 ohmically heated L-mode plasmas with stationary line-average core density of $\overline{n}_e/n_G = 0.12$, 0.28, and 0.42, where the MLPs sample that plasma at the limiter radius $\rho \approx 1.5$ cm is analyzed. The length of the acquired data time series is between 0.7 and 1.5 s. Table 1 lists the mean and root-mean square value of the electron density, temperature and velocity and Fig. 11 shows equi-probability contours for joint PDFs of the density, temperature, and velocity fluctuations respectively. The line-averaged core plasma density is color coded as before and the equi-probability contours are labelled with their respective probability.

Electron density and temperature fluctuations appear strongly correlated in all three discharges, as suggested by the small minor axis of the ellipsoid equi-probability contours shown in Fig. 11a. Linear Pearson sample correlation coefficients are given by $R = 0.79$, $R = 0.89$ and $R = 0.90$ for the three discharges. Notably, the discharge with $\overline{n}_e/n_G = 0.46$ shows a lack of temperature fluctuations with $\tilde{T}_e \lesssim -1.5$ due to the low average temperature and an abundance of large-amplitude temperature fluctuations. The range of the electron density fluctuations changes only little with $\overline{n}_e/n_G$.

The joint PDF of $\tilde{U}$ and $\tilde{n}_e$ suggests a smaller level of correlation between density and velocity fluctuations. For $\tilde{n} > 0$, the measured velocity fluctuations are on average positive, however with a larger scatter than observed for the temperature fluctuations. Likewise, fluctuations with $\tilde{U} > 0$ are on average recorded simultaneously with fluctuations for which $\tilde{n}_e > 0$. The shape of the joint PDF is similar for all three discharges. In the high-density discharge, $\overline{n}_e/n_G = 0.46$, density fluctuations with $\tilde{n}_e \approx 2$ appear in phase with slightly larger velocity fluctuations as is the case for the two discharges with lower density.

Joint PDFs of fluctuations of the electron temperature and the velocity, presented in Fig. 11c, feature a similar shape as the joint PDF of $\tilde{U}$ and $\tilde{n}_e$. On average, fluctuations with $\tilde{T}_e > 0$ are recorded simultaneously with $\tilde{U} > 0$ and fluctuations with $\tilde{T}_e < 0$ are recorded simultaneously with $\tilde{U} < 0$. Compared to the low density discharges, the qualitative picture of the correlations observed in the high-density discharge changes only little. Fewer samples with negative $\tilde{T}_e$ are recorded due to the lower average electron temperature in this discharge.

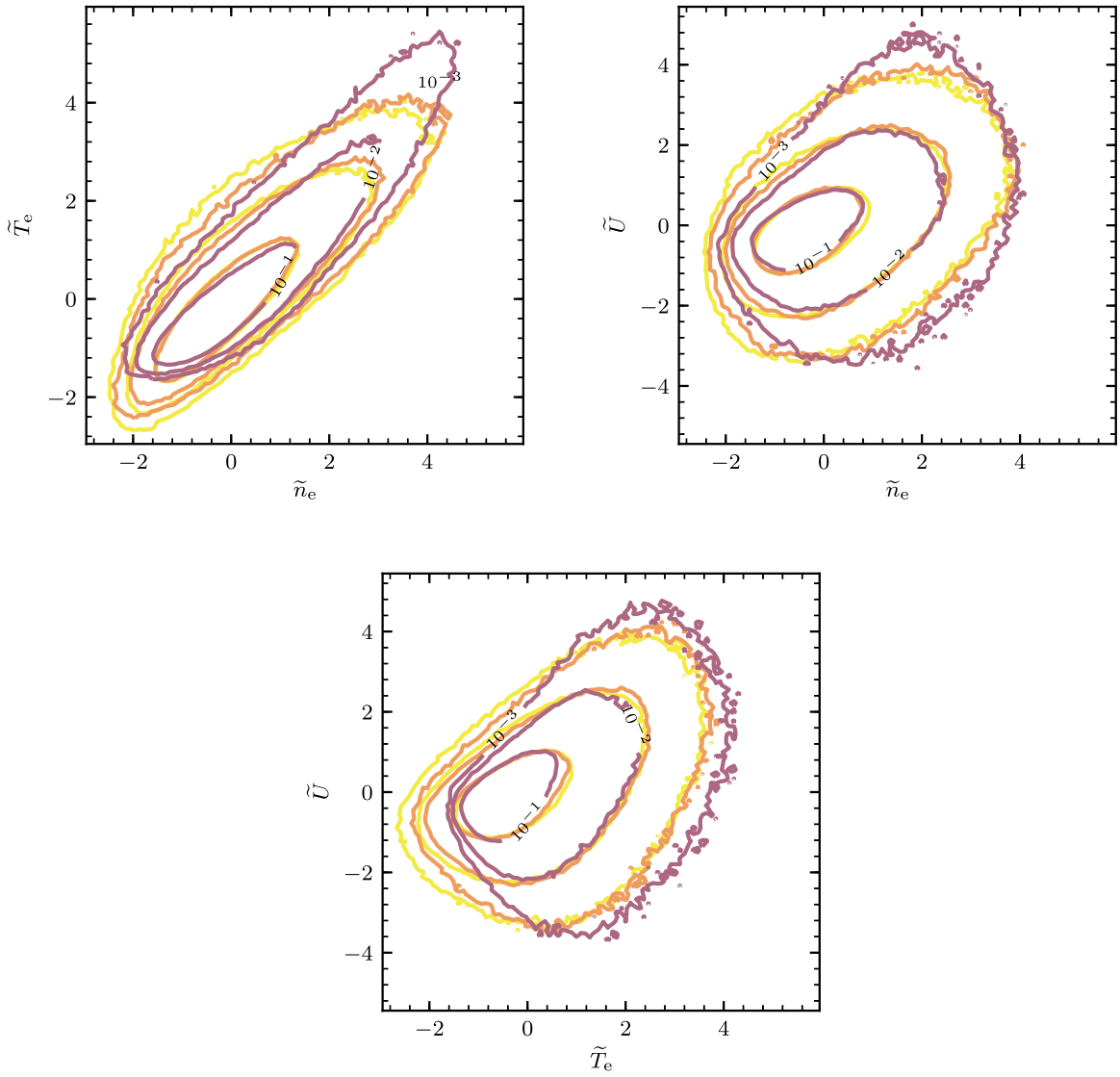

Fig. 11. Joint PDFs of the electron density, temperature and radial velocity fluctuations.

Table 1
Sample averaged and root-mean-square values for the fluctuations presented in Fig. 11. The upper, middle, and lower value refer to the densities $\overline{n}_e/n_G = 0.12$, 0.28, and 0.46 shown in Fig. 11.

	mean	rms
$n_e/10^{18}\mathrm{m}^{-3}$	8.46 / 18.7 / 48.0	1.68 / 4.49 / 10.3
T_e/eV	16.7 / 15.0 / 13.4	2.22 / 3.17 / 5.21
U/ms^{-1}	0 / 0 / 0	367 / 476 / 453

4. Discussion and conclusion

Revisiting profile flattening using real-time data of the electron density and temperature allows to distinguish which one of these quantities determines effects observed in the fluctuation statistics of the ion saturation current, assuming $I_s \sim n_e T_e^{1/2}$. Firstly, with increasing line-averaged core plasma density, the break point of the $\langle n_e \rangle$ profile moves closer to the separatrix while the scale lengths L_n and L_f increase. The break point of the $\langle T_e \rangle$ profile also moves radially inwards, but remains farther away from the separatrix. This suggests that the broadening of the $\langle I_s \rangle$ profile is governed by the development of a shoulder in the $\langle n_e \rangle$ profile. Secondly, the relative fluctuation level of the particle density remains constant with $\overline{n}_e/n_G$ while the relative fluctuation level of the temperature increases. This implies that the increase of the I_s relative fluctuation level is governed the electron temperature fluctuations. Thirdly, in discharges with $\overline{n}_e/n_G \lesssim 0.3$, the magnitude of the sample skewness and excess kurtosis shows no significant variation for either I_s, n_e, and T_e with $\overline{n}_e/n_G$ and ρ. In the discharge with $\overline{n}_e/n_G = 0.45$, S and F calculated from the I_s and T_e samples are significantly larger than values found in the low density discharges. For the electron density, S and F appear independent of the line-averaged core-plasma density.

Estimating the radial electric drift velocity using either V_f and V_p yields comparable values in discharges with $\overline{n}_e/n_G \lesssim 0.3$. In higher density discharges the estimator using V_p yields significantly larger radial velocities. An increase in radial blob velocities in high-density plasma discharges is well documented for Alcator C-Mod and ASDEX Upgrade [8,23–25]. In the high-density discharges, both S and F are well above sample estimates found in low-density discharges. This implies that the $\tilde{U}$ data feature a large number of samples which are significantly larger than the sample average. The line-averaged core density separates $S(U_{V_p})$ and $F(U_{V_p})$ similarly to $S(T_e)$ and $F(T_e)$. Since the plasma potential is estimated as $V_p = V_f + \Lambda T_e$, with $\Lambda \approx 3$, see [1], the increase in $S(U_{V_p})$ and $F(U_{V_p})$ with $\overline{n}_e/n_G$ may be due to more frequent T_e fluctuations with small perpendicular wave numbers.

It is interesting to analyze the observed average density profiles

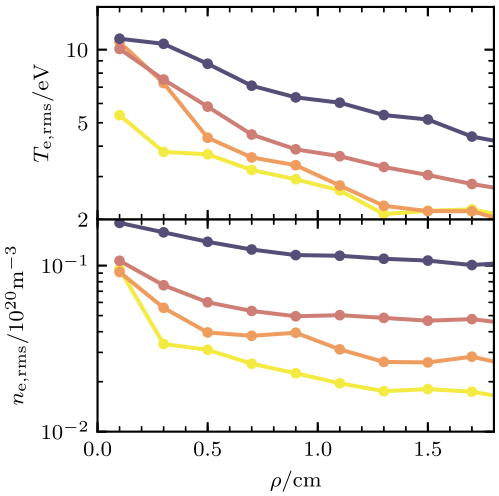

Fig. 12. Radial profiles of the absolute root-mean-square values of the electron temperature (upper panel) and the electron density (lower panel).

using a stochastic model that describes the SOL plasma as the superposition of radially outwards propagating pulses [26,49]. Adapting this point of view, the radial profile scale is given by $L_\perp = v_\perp \tau_{||}$. Here, $v_\perp$ is the radial velocity of the individual pulses and $\tau_{||}$ describes parallel losses along the magnetic field due to acoustic streaming. This streaming can be assumed to occur at the ion acoustic velocity, $C_s = \sqrt{T_e/m_i}$. Then the radial velocity can be estimated as $C_s L_\perp / L_{||}$, where $L_{||} = 10$m. Using $L_\perp = 3$cm and $T_e = 30$eV for the low density discharges, $\bar{n}_e/n_G \lesssim 0.3$, this yields $v_\perp \approx 100 \text{ms}^{-1}$. Using $L_\perp = 6$cm and $T_e = 20$eV for the high density discharge, $\bar{n}_e/n_G \approx 0.4$, this yields $v_\perp \approx 200 \text{ms}^{-1}$. These increasing estimates of $v_\perp$ are compatible with the order of magnitude estimated U_{rms} in the respective discharges. The values estimated for $v_\perp$ as well as the trend that $v_\perp$ increases with increasing line-averaged core plasma density are furthermore compatible with estimates of the radial blob velocity in similar Alcator C-Mod plasmas obtained by Langmuir probe measurements [50], obtained by tracking of blob structures using gas-puff imaging measurements [24], and obtained by correlation methods of the convective velocity field [23,51].

In discharges with $\bar{n}_e/n_G \lesssim 0.3$, the convective heat flux, driven by electron density fluctuations, dominates the total fluctuation driven heat flux. In the discharge with $\bar{n}_e/n_G = 0.45$, this contribution is reduced to approximately 35%, while the contribution from the conductive heat flux is approximately 50%. Given the definition of the heat fluxes in Eq. 3, this switching may be due to either a change in the fluctuation amplitudes or a change in the average profiles. As discussed at end of the last section, the joint PDFs suggest that there is little change in the phase of the density, temperature, and velocity fluctuations.

As shown in Fig. 12, the absolute root-mean-square value of the electron density is more sensitive to variations in $\bar{n}_e/n_G$ than the root-mean-square value of the electron temperature. For example at $\rho = 0.7$cm we find that $n_{e,\,rms}$ increases by a factor of 5, from $2.5 \times 10^{18}\,\text{m}^3$ for $\bar{n}_e/n_G = 0.12$ to approximately $1.2 \times 10^{19}\,\text{m}^3$ for $\bar{n}_e/n_G = 0.45$. On the other hand, $T_{e,\,rms}$ increases from 3.3 eV to 7eV. Furthermore, the correlations between $\tilde{U}$, $\tilde{n}_e$ and $\tilde{T}_e$ change little with $\bar{n}_e/n_G$. Putting these pieces together, the following picture emerges: In low density discharges, a large average electron temperature, together with large-amplitude electron density fluctuations govern the radial heat flux. Contributions from triple correlations are almost negligible. In the high density discharge, a large average electron density, together with large-amplitude electron temperature fluctuations govern the radial heat flux. The convective heat flux, and contributions from triple correlations are secondary but not negligible. Finally, the near-SOL lengths scales L_n of the n_e and T_e profiles change little in the observed range of line-averaged core plasma compared to the average radial particle and heat fluxes, which increase by several orders of magnitude. This corroborates the idea that the profile gradients do not drive particle and energy fluxes [37,38,49].

The analysis of the presented discharges suggests a clear correlation between the fluctuation statistics of the thermodynamic variables, the radial electric drift velocity, as well as the particle and heat fluxes and the line-averaged core plasma density. The absolute magnitude of the electron density, velocity, and particle and heat-flux fluctuations are significantly smaller in low density discharges, $\bar{n}_e/n_G \lesssim 0.3$ than in the high-density discharge $\bar{n}_e/n_G = 0.45$. However, the absolute magnitude of the electron temperature fluctuations changes only little with $\bar{n}_e/n_G$. This critical line-averaged core plasma density separates the regimes where the conductive and the convective heat fluxes respectively govern the radial heat transport in the outboard mid-plane SOL. While this transition coincides with the threshold for divertor detachment, at approximately $\bar{n}_e/n_G = 0.4$, the data presented here do not allow to draw conclusions about any causal links to the downstream conditions. Rather, the data highlights the role of the boundary conditions imposed on the SOL plasma at the separatrix. Within the studied range of line-averaged core plasma densities, $\langle n_e(\rho = 0)\rangle$ increases by a factor of two, while $\langle T_e(\rho = 0)\rangle$ decreases by a factor of three. The observed flux switching from conduction to convection dominated is found to correlate with a significant increase/decrease in the separatrix values of the average profiles. This suggests that it is the fluctuation-driven transport in combination with the parallel transport which sets the gradient scale lengths in the SOL.

In future work, MLP measurements of scrape-off-layer fluctuations will be interpreted in terms of a stochastic model which describes the fluctuations by the super-position of uncorrelated pulses. It is also planned to address the interplay between ionization and the observed change in profiles.

Acknowledgements

This work was supported with financial subvention from the Research Council of Norway under Grant No. 240510/F20 and from the U.S. DoE under Cooperative Agreement No. DE-FC02-99ER54512 using the Alcator C-Mod tokamak, a DoE Office of Science user facility. R. K. , O. E. G., and A. T. acknowledge the generous hospitality of the MIT Plasma Science and Fusion Center during a research stay where this work has been performed.

References

[1] P.C. Stangeby, The plasma boundary of magnetic fusion devices, IoP Publishing, 2000.
[2] S.I. Itoh, K. Itoh, On scaling laws in scrape-off-layer plasmas, Plasma Phys. Control. Fusion 36 (11) (1994) 1845.
[3] G. Counsell, J. Connor, S. Erents, A. Field, S. Fielding, B.L. Bombard, K. Morel, Sol width scaling from consideration of edge transport in tokamaks, J. Nucl. Mater. 266–269 (1999) 91–98, https://doi.org/10.1016/S0022-3115(98)00880-0.
[4] B. LaBombard, R.L. Boivin, M. Greenwald, J. Hughes, B. Lipschultz, D. Mossessian, C.S. Pitcher, J.L. Terry, S.J. Zweben, the Alcator C-Mod Group, Particle transport in the scrape-off layer and its relationship to discharge density limit in alcator c-mod, Phys. Plasmas 8 (5) (2001) 2107–2117, https://doi.org/10.1063/1.1352596.
[5] J.A. Boedo, D. Rudakov, R. Moyer, S. Krasheninnikov, D. Whyte, G. McKee, G. Tynan, M. Schaffer, P. Stangeby, P. West, S. Allen, T. Evans, R. Fonck, E. Hollmann, A. Leonard, A. Mahdavi, G. Porter, M. Tillack, G. Antar, Transport by intermittent convection in the boundary of the diii-d tokamak, Phys. Plasmas 8 (11) (2001) 4826–4833, https://doi.org/10.1063/1.1406940.
[6] D. Rudakov, J. Boedo, R. Moyer, P. Stangeby, J. Watkins, D. Whyte, L. Zeng, N. Brooks, R. Doerner, T. Evans, M. Fenstermacher, M. Groth, E. Hollmann, S. Krasheninnikov, C. Lasnier, A. Leonard, M. Mahdavi, G. McKee, A. McLean, A. Pigarov, W. Wampler, G. Wang, W. West, C. Wong, Far sol transport and main wall plasma interaction in diii-d, Nucl. Fusion 45 (12) (2005) 1589.
[7] O.E. Garcia, R.A. Pitts, J. Horacek, J. Madsen, V. Naulin, A.H. Nielsen, J.J. Rasmussen, Collisionality dependent transport in tcv sol plasmas, Plasma Phys. Control. Fusion 49 (12B) (2007) B47.
[8] D. Carralero, G. Birkenmeier, H. Müller, P. Manz, P. deMarne, S. Müller, F. Reimold,

U. Stroth, M. Wischmeier, E. Wolfrum, T.A.U. Team, An experimental investigation of the high density transition of the scrape-off layer transport in asdex upgrade, Nucl. Fusion 54 (12) (2014) 123005.
[9] L. Spitzer, R. Härm, Transport phenomena in a completely ionized gas, Phys. Rev. 89 (1953) 977–981, https://doi.org/10.1103/PhysRev.89.977.
[10] W. Fundamenski, W. Sailer, J.E. contributors, Radial propagation of type-i elms on jet, Plasma Phys. Control. Fusion 46 (1) (2004) 233.
[11] G.Y. Antar, S.I. Krasheninnikov, P. Devynck, R.P. Doerner, E.M. Hollmann, J.A. Boedo, S.C. Luckhardt, R.W. Conn, Experimental evidence of intermittent convection in the edge of magnetic confinement devices, Phys. Rev. Lett. 87 (2001) 065001, https://doi.org/10.1103/PhysRevLett.87.065001.
[12] S.I. Krasheninnikov, On scrape off layer plasma transport, Phys. Lett. A 283 (5–6) (2001) 368–370, https://doi.org/10.1016/S0375-9601(01)00252-3.
[13] D.A. D'Ippolito, J.R. Myra, S.I. Krasheninnikov, Cross-field blob transport in tokamak scrape-off-layer plasmas, Phys. Plasmas 9 (1) (2002) 222–233, https://doi.org/10.1063/1.1426394.
[14] D.A. D'Ippolito, J.R. Myra, S.J. Zweben, Convective transport by intermittent blob-filaments: comparison of theory and experiment, Phys. Plasmas 18 (6) (2011) 060501, https://doi.org/10.1063/1.3594609.
[15] O.E. Garcia, N.H. Bian, W. Fundamenski, Radial interchange motions of plasma filaments, Phys. Plasmas 13 (8) (2006) 082309, https://doi.org/10.1063/1.2336422.
[16] C. Theiler, I. Furno, P. Ricci, A. Fasoli, B. Labit, S.H. Müller, G. Plyushchev, Cross-field motion of plasma blobs in an open magnetic field line configuration, Phys. Rev. Lett. 103 (6) (2009) 065001, https://doi.org/10.1103/PhysRevLett.103.065001.
[17] R. Kube, O.E. Garcia, Velocity scaling for filament motion in scrape-off layer plasmas, Phys. Plasmas 18 (10) (2011), https://doi.org/10.1063/1.3647553.
[18] M. Wiesenberger, J. Madsen, A. Kendl, Radial convection of finite ion temperature, high amplitude plasma blobs, Phys. Plasmas 21 (9) (2014), https://doi.org/10.1063/1.4894220.
[19] M. Held, M. Wiesenberger, J. Madsen, A. Kendl, The influence of temperature dynamics and dynamic finite ion larmor radius effects on seeded high amplitude plasma blobs, Nucl. Fusion 56 (12) (2016) 126005.
[20] J. Olsen, J. Madsen, A.H. Nielsen, J.J. Rasmussen, V. Naulin, Temperature dynamics and velocity scaling laws for interchange driven, warm ion plasma filaments, Plasma Phys. Control. Fusion 58 (4) (2016) 044011.
[21] J.R. Myra, D.A. Russell, D.A. D'Ippolito, Collisionality and magnetic geometry effects on tokamak edge turbulent transport. i. a two-region model with application to blobs, Phys. Plasmas 13 (11) (2006) 112502, https://doi.org/10.1063/1.2364858.
[22] L. Easy, F. Militello, J. Omotani, N.R. Walkden, B. Dudson, Investigation of the effect of resistivity on scrape off layer filaments using three-dimensional simulations, Phys. Plasmas 23 (1) (2016) 012512, https://doi.org/10.1063/1.4940330.
[23] M. Agostini, J. Terry, P. Scarin, S. Zweben, Edge turbulence in different density regimes in alcator c-mod experiment, Nucl. Fusion 51 (5) (2011) 053020.
[24] R. Kube, O. Garcia, B. LaBombard, J. Terry, S. Zweben, Blob sizes and velocities in the alcator c-mod scrape-off layer, J. Nucl. Mater. 438, Supplement (0) (2013) S505–S508, https://doi.org/10.1016/j.jnucmat.2013.01.104.
[25] D. Carralero, M. Siccinio, M. Komm, S. Artene, F. D'Isa, J. Adamek, L. Aho-Mantila, G. Birkenmeier, M. Brix, G. Fuchert, M. Groth, T. Lunt, P. Manz, J. Madsen, S. Marsen, H. Müller, U. Stroth, H. Sun, N. Vianello, M. Wischmeier, E. Wolfrum, A.U. Team, C. Team, J. Contributors, T.E.M. Team, Recent progress towards a quantitative description of filamentary sol transport, Nucl. Fusion 57 (5) (2017) 056044.
[26] O.E. Garcia, Stochastic modeling of intermittent scrape-off layer plasma fluctuations, Phys. Rev. Lett. 108 (2012) 265001, https://doi.org/10.1103/PhysRevLett.108.265001.
[27] O.E. Garcia, S.M. Fritzner, R. Kube, I. Cziegler, B. LaBombard, J.L. Terry, Intermittent fluctuations in the alcator c-mod scrape-off layer, Phys. Plasmas 20 (2013) 055901.
[28] A. Theodorsen, O.E. Garcia, J. Horacek, R. Kube, R.A. Pitts, Scrape-off layer turbulence in tcv: evidence in support of stochastic modelling, Plasma Phys. Control. Fusion 58 (4) (2016) 044006.
[29] O.E. Garcia, R. Kube, A. Theodorsen, J.-G. Bak, S.-H. Hong, H.-S. Kim, the KSTAR Project Team, R. Pitts, {SOL} Width and intermittent fluctuations in {KSTAR}, Nucl. Mat. Energy (2016), https://doi.org/10.1016/j.nme.2016.11.008.
[30] A. Theodorsen, O. Garcia, R. Kube, B. LaBombard, J. Terry, Relationship between frequency power spectra and intermittent, large-amplitude bursts in the alcator c-mod scrape-off layer, Nucl. Fusion 57 (11) (2017) 114004.
[31] R. Kube, O.E. Garcia, A. Theodorsen, D. Brunner, A.Q. Kuang, B. LaBombard, J.L. Terry, Intermittent electron density and temperature fluctuations and associated fluxes in the alcator c-mod scrape-off layer, Plasma Phys. Control. Fusion 60 (6) (2018) 065002.
[32] O.E. Garcia, R. Kube, A. Theodorsen, B. LaBombard, J.L. Terry, Intermittent fluctuations in the alcator c-mod scrape-off layer for ohmic and high confinement mode plasmas, Phys. Plasmas 25 (5) (2018) 056103, https://doi.org/10.1063/1.5018709.
[33] O.E. Garcia, J. Horacek, R.A. Pitts, A.H. Nielsen, W. Fundamenski, V. Naulin, J.J. Rasmussen, Fluctuations and transport in the tcv scrape-off layer, Nucl. Fusion 47 (7) (2007) 667.
[34] P. Ricci, F.D. Halpern, S. Jolliet, J. Loizu, A. Mosetto, A. Fasoli, I. Furno, C. Theiler, Simulation of plasma turbulence in scrape-off layer conditions: the gbs code, simulation results and code validation, Plasma Phys. Control. Fusion 54 (12) (2012) 124047.
[35] P. Tamain, H. Bufferand, G. Ciraolo, C. Colin, D. Galassi, P. Ghendrih, F. Schwander, E. Serre, The tokam3x code for edge turbulence fluid simulations of tokamak plasmas in versatile magnetic geometries, J. Comput. Phys. 321 (2016) 606–623, https://doi.org/10.1016/j.jcp.2016.05.038.
[36] Y. Marandet, H. Bufferand, N. Nace, M. Valentinuzzi, G. Ciraolo, P. Tamain, J. Bucalossi, D. Galassi, P. Ghendrih, N. Mellet, E. Serre, Towards a consistent modelling of plasma edge turbulence in mean field transport codes: focus on sputtering and plasma fluctuations, Nucl. Mat. Energy 12 (2017) 931–934, https://doi.org/10.1016/j.nme.2017.02.007. Proceedings of the 22nd International Conference on Plasma Surface Interactions 2016, 22nd PSI.
[37] B. LaBombard, J. Hughes, D. Mossessian, M. Greenwald, B. Lipschultz, J. Terry, the Alcator C-Mod Team, Evidence for electromagnetic fluid drift turbulence controlling the edge plasma state in the alcator c-mod tokamak, Nucl. Fusion 45 (12) (2005) 1658.
[38] B. LaBombard, J.W. Hughes, N. Smick, A. Graf, K. Marr, R. McDermott, M. Reinke, M. Greenwald, B. Lipschultz, J.L. Terry, D.G. Whyte, S.J. Zweben, Critical gradients and plasma flows in the edge plasma of alcator c-mod, Phys. Plasmas 15 (5) (2008) 056106, https://doi.org/10.1063/1.2838246.
[39] A. Wynn, B. Lipschultz, I. Cziegler, J. Harrison, A. Jaervinen, G.F. Matthews, J. Schmitz, B. Tal, M. Brix, C. Guillemaut, D. Frigione, A. Huber, E. Joffrin, U. Kruzei, F. Militello, A. Nielsen, N. Walkden, S. Wiesen, J. Contributors, Investigation into the formation of the scrape-off layer density shoulder in jet iter-like wall l-mode and h-mode plasmas, Nucl. Fusion 58 (5) (2018) 056001.
[40] M. Greenwald, Density limits in toroidal plasmas, Plasma Phys. Control. Fusion 44 (8) (2002) R27.
[41] L. Lao, H.S. John, R. Stambaugh, A. Kellman, W. Pfeiffer, Reconstruction of current profile parameters and plasma shapes in tokamaks, Nucl. Fusion 25 (11) (1985) 1611.
[42] D. Brunner, A.Q. Kuang, B. LaBombard, W. Burke, Linear servomotor probe drive system with real-time self-adaptive position control for the alcator c-mod tokamak, Rev. Sci. Instrum. 88 (7) (2017) 073501, https://doi.org/10.1063/1.4990043.
[43] N. Smick, B. LaBombard, Wall scanning probe for high-field side plasma measurements on alcator c-mod, Rev. Sci. Instrum. 80 (2) (2009), https://doi.org/10.1063/1.3069290.
[44] B. Labombard, L. Lyons, Mirror langmuir probe: a technique for real-time measurement of magnetized plasma conditions using a single langmuir electrode, Rev. Sci. Instrum. 78 (7) (2007) 073501–073501–9, , https://doi.org/10.1063/1.2754392.
[45] B. LaBombard, T. Golfinopoulos, J.L. Terry, D. Brunner, E. Davis, M. Greenwald, J.W. Hughes, New insights on boundary plasma turbulence and the quasi-coherent mode in alcator c-mod using a mirror langmuir probe, Phys. Plasmas 21 (5) (2014) 056108, https://doi.org/10.1063/1.4873918.
[46] H. Müller, J. Adamek, J. Horacek, C. Ionita, F. Mehlmann, V. Rohde, R. Schrittwieser, A.U. Team, Towards fast measurement of the electron temperature in the sol of asdex upgrade using swept langmuir probes, Contrib. Plasma Phys. 50 (9) (2010) 847–853, https://doi.org/10.1002/ctpp.201010144.
[47] O. Garcia, R. Pitts, J. Horacek, A. Nielsen, W. Fundamenski, J. Graves, V. Naulin, J.J. Rasmussen, Turbulent transport in the {TCV} {SOL}, J. Nucl. Mater. 363–365 (2007) 575–580, https://doi.org/10.1016/j.jnucmat.2006.12.063.
[48] J. Goetz, B. Lipschultz, M. Graf, C. Kurz, R. Nachtrieb, J. Snipes, J. Terry, Power balance and scaling of the radiated power in the divertor and main plasma of alcator c-mod, J. Nucl. Mater. 220–222 (1995) 971–975. Plasma-Surface Interactions in Controlled Fusion Devices. doi:10.1016/0022-3115(94)00456-0 .
[49] O.E. Garcia, R. Kube, A. Theodorsen, H.L. Pécseli, Stochastic modelling of intermittent fluctuations in the scrape-off layer: correlations, distributions, level crossings, and moment estimation, Phys. Plasmas 23 (5) (2016) 052308, https://doi.org/10.1063/1.4951016.
[50] R. Kube, A. Theodorsen, O.E. Garcia, B. LaBombard, J.L. Terry, Fluctuation statistics in the scrape-off layer of alcator c-mod, Plasma Phys. Control. Fusion 58 (5) (2016) 054001.
[51] J. Terry, N. Basse, I. Cziegler, M. Greenwald, O. Grulke, B. LaBombard, S. Zweben, E. Edlund, J. Hughes, L. Lin, Y. Lin, M. Porkolab, M. Sampsell, B. Veto, S. Wukitch, Transport phenomena in the edge of alcator c-mod plasmas, Nucl. Fusion 45 (11) (2005) 1321.